Pretreatment for Water Reuse using Fluidized Bed Crystallization

Mojtaba AzadiAghdam, Minkyu Park, Israel J. Lopez-Prieto, Andrea Achilli, Shane A. Snyder, James Farrell*

University of Arizona, Department of Chemical and Environmental Engineering

1133 E. James E. Rogers Way, Tucson, AZ 85721, USA

*Corresponding author: James Farrell, Email: farrellj@email.arizona.edu

Abstract

This research investigated the use of fluidized bed crystallization for removing scale forming species and natural organic matter (NOM) from treated municipal wastewater prior to water reclamation. The effect of pH on Ca^{2+}, Mg^{2+}, silica and NOM removal in a fluidized bed crystallization reactor (FBCR) was determined. NOM removal in the FBCR was compared to that for the conventional treatments, ultrafiltration and ferric chloride coagulation/flocculation. Under optimized conditions, fluidized bed crystallization was able to remove more than 99.9% of Mg^{2+}, 97% of Ca^{2+} and 42% of silica. The FBCR was also able to remove 25% of NOM, which was intermediate between NOM removal by ferric chloride (56%) and ultrafiltration (13%). Size exclusion chromatography-organic carbon detection (SEC-OCD) indicated that the majority of NOM removal occurred via co-precipitation with $Mg(OH)_2$. Excitation emission matrix-parallel factor (EEM-PARAFAC) analysis was used to investigate the types of NOM removed. The FBCR was able to remove all five NOM components (three humic acids, one fulvic acid and one protein-like substance), including 100% of the autochthonous fulvic acids. Ferric chloride was also able to remove all five NOM components, but only one third of the autochthonous fulvic acids, while ultrafiltration was able to remove only 11% of the protein-like NOM.

Keywords: Fluidized bed crystallization, Ultrafiltration, Ferric chloride coagulation and flocculation, Excitation emission matrix, parallel factor analysis

1. Introduction

Potable water scarcity has become an important issue over the last few decades due to changes in rainfall patterns and increasing population. Recent estimates indicate that over one billion people do not have access to clean, potable water, and approximately 2.3 billion people live in regions with water shortages [i]. Thus, water reuse and recycling are becoming increasingly necessary to augment potable water supplies [ii].

High pressure membrane processes, such as nanofiltration (NF) and reverse osmosis (RO), are commonly used to produce drinking water from various water sources, such as seawater, brackish water, and surface water. These membrane processes may also be used for converting municipally treated wastewater into potable water [iii]. However, there are additional challenges in treating secondary effluent wastewater to potable quality [iv]. Secondary effluent wastewater contains a more complex mixture of organic matter than most sources of brackish water, which contain mostly plant derived humic and fulvic acids. Treated municipal wastewater contains significant concentrations of microbial proteins and extracelluar polysaccharides that have high membrane fouling potential. Thus, prior to membrane treatment, secondary effluent wastewater may require more extensive pretreatment than most brackish waters.

The goal of pretreatment processes is to obtain the highest level of foulant removal that makes downstream membrane processes technically and economically feasible. This will increase water recovery and reduce the volume of concentrate requiring further treatment or disposal. Contributions to membrane fouling include: 1) active and inactive microorganisms; 2) adsorbed colloidal material; 3) precipitated mineral scale, most commonly divalent cations

combined with carbonate or sulfate; and 4) adsorbed natural organic matter (NOM), such as humic and fulvic acids. Treatment methods for removing membrane foulants include: 1) precipitation processes, such as lime softening or fluidized bed crystallization; 2) coagulation/flocculation processes using iron or aluminum coagulants; and 3) membrane processes, such as ultrafiltration.

Precipitation processes primarily remove inorganic minerals, such as $CaCO_3$, $Mg(OH)_2$, and $MgO(SiO_2)_x \cdot (H_2O)_x$, that are precipitated at elevated pH values [v,vi]. In conventional precipitation softening, the maximum pH value is normally kept below 10.5 in order avoid precipitation of $Mg(OH)_2$, which has unfavorable settling behavior [vii]. The use of fluidized bed crystallization for Mg^{2+} removal avoids the settling problems associated with $Mg(OH)_2$ precipitation, and also requires lower dosages of pH adjusting chemicals than traditional precipitation processes [5]. Fluidized bed crystallization reactors (FBCRs) are seeded with sand or other mineral grains that serve as nucleation sites for precipitation of hardness minerals. Upward flow through the reactor fluidizes the seed bed while injection of an alkaline chemical increases the pH of the solution, thereby promoting heterogeneous precipitation on the seed particles. Heterogeneous precipitation is faster than homogeneous nucleation, and requires lower levels of supersaturation to precipitate hardness minerals [5]. This means that for similar calcium and magnesium removal, less chemical addition is needed for a FBCR compared to conventional softening. The typical hydraulic residence time in a FBCR is less than 30 seconds, while the mixing time in conventional softening can take up to 120 min [viii]. Conventional softening produces relatively small crystals due to homogeneous formation of many crystal nuclei. This makes the

solid-liquid separation process difficult, since the produced sludge is difficult to dewater [ix]. In contrast, FBCRs produce large particulates with fast settling velocities. This leads to particle size classification along the length of the fluidized bed, with the largest particles settling to the bottom of the reactor. These large particles are periodically flushed from the reactor, and are easily dewatered due to their large size (>5 mm) [5].

Coagulation and flocculation are cost-effective conventional treatments that are often used prior to high-pressure membrane filtration processes. Coagulation is able to effectively remove acidic and hydrophobic organic compounds, macromolecules, colloidal particles and suspended solids [x]. As conventional coagulants, ferric or aluminum salts destabilize colloidal particles and provide a high specific surface area for adsorption of organic matter and multivalent cations. The most important parameters for an optimized coagulation process are the type of coagulant, dose and resulting pH value.

Ultrafiltration (UF) is becoming an increasingly used pretreatment for RO, due to its high removal of suspended and colloidal contaminants. UF operates as a physical barrier with pore sizes ranging from 0.002 to 0.1 µm, and it is able to achieve over 4 log removal of pathogens, such as Giardia and Cryptosporidium [xi]. In UF systems, turbidity and SDI_{15} can be lowered to less than 0.1 NTU and 3, respectively [xii,xiii]. However, UF removes only small amounts of dissolved organic matter, mostly due to physical adsorption on the membrane.

In this study, fluidized bed crystallization was used to remove mineral solids and NOM from treated municipal wastewater. While there are numerous studies on using softening as a pre-treatment for high-pressure membrane filtration processes [4,6,8, xiv,xv,xvi], there are no studies

on treating secondary effluent using a FBCR. Precipitation of both mineral solids and NOM in a FBCR may differ significantly from that observed in a typical lime-soda ash softening process. The pH gradient and absence of homogeneous nucleation in a FBCR may affect the levels of hardness and NOM removal compared to conventional softening, which has practical limits of 0.6 meq/L for Ca^{2+} and 0.2 meq/L for Mg^{2+} [7]. For NOM removal via conventional softening, $CaCO_3$ precipitation removes 10-30%, while $Mg(OH)_2$ precipitation can achieve an additional 30-60% [ ]. In conventional softening, the small crystal size and its associated high specific surface area helps promote hydrophobic NOM removal by physical adsorption. It is unknown how the larger particles produced during fluidized bed crystallization will affect NOM removal. If fluidized bed crystallization can achieve substantial NOM removal, in addition to hardness ion removal, it may prove to be a superior pretreatment for reverse osmosis than conventional UF or ferric chloride.

In this research, hardness minerals and NOM removal from treated municipal wastewater was measured in a FBCR operating with effluent pH values ranging from 10.5 to 12. The types of NOM removal in the FBCR were determined via excitation emission matrix (EEM) and EEM-parallel factor analysis (PARAFAC). Size exclusion chromatography-organic carbon detection (SEC-OCD) was used to investigate the co-precipitation of inorganic and organic contaminants. NOM removal in the FBCR was compared to conventional treatment using UF or ferric chloride.

2. Materials and Methods

2.1 Treated Wastewater

Effluent water from the secondary clarifier at the Agua Nueva water reclamation facility was piped to the co-located Water and Energy Sustainable Technology (WEST) Center in Tucson,

Arizona. Wastewater at The Agua Nueva water reclamation facility is treated with dissolved air flotation, a 5-stage Bardenpho biological process, final clarification, disk filtration, and chlorination. Details of its typical water quality are shown in Table 1.

Table 1. Properties of secondary effluent wastewater.

Parameters	*Concentration (mg/L)*
pH	7.2-7.5
Turbidity (NTU)	0.8-1.2
Alkalinity (as $CaCO_3$)	153-203
Sodium	143-149
Magnesium	15-18
Potassium	16-18
Calcium	87-97
Barium	0.1-0.3
Chloride	134-140
Bromide	0.3-0.5
Sulfate	177-182
Silica	35.3-39.6

2.2 Materials

Powdered sodium hydroxide, 37% hydrochloric acid, and 40% ferric chloride solutions were procured from Hill Brothers Chemical Company (Tucson, Arizona, USA). Garnet sand (#60) for the FBCR was procured from Red Flint Sand & Gravel, LLC (Eau Claire, Wisconsin, USA).

2.3 Equipment

The FBCR reactor consisted of a 280 cm tall by 15.24 cm internal diameter, clear PVC pipe housing a 150 cm long bed of garnet sand. The secondary effluent was fed into the bottom of the pipe and a 0.1 M sodium hydroxide solution was injected into the FBCR from four equally-spaced injection ports along the length of the bed, as illustrated in Figure 1. The secondary effluent flow

rate was 1.5 L/min, which produced a 20-25% bed expansion. Effluent from the FBCR was passed through a 50 cm-long polypropylene Aquaboon 5 µm filter contained in a standard filter housing.

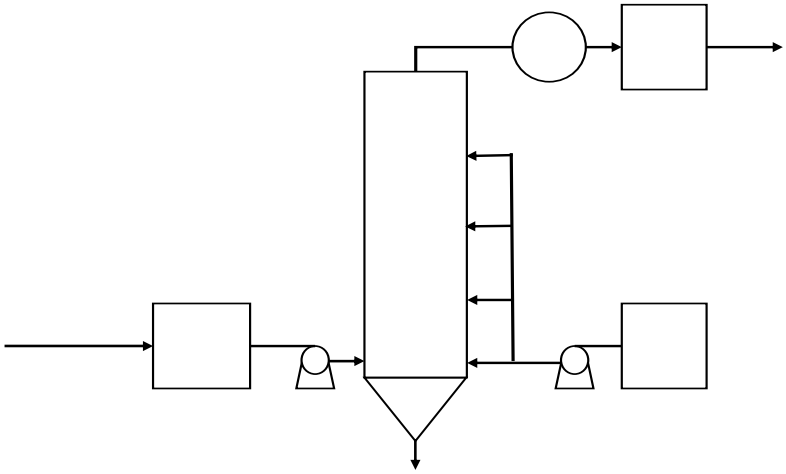

Figure 1. Schematic diagram of the fluidized-bed crystallization system.

A full-scale UF system using a DOW IntegraFlux UXA-2680XP module with a nominal pore diameter of 0.03 µm was procured from Applied Membranes Inc. (Vista, California, USA). At the time of this study, the UF system was being used as pretreatment for a full-scale RO system, and had been operating continuously for 18 months. The combined UF/RO process has averaged 60% recovery, and required weekly cleaning with acid and caustic solutions.

Ferric chloride coagulation and flocculation experiments were conducted using a jar test apparatus (PB-900 Programmable Jar tester, Phipps & Bird) containing 6 reaction vessels. The dimensions of the vessels were 11.5 cm × 11.5 cm × 21 cm, and each test was conducted with 1 liter of solution. Solutions were mixed at 250 rpm for 3 min immediately after dosing with ferric chloride, and then the mixing rate was reduced to 50 rpm for a 20 or 30 min flocculation period. Precipitates in the solutions were left to settle for 30 min prior to sampling from the supernatant.

2.4 Analytical Methods

Anions were analyzed using ion chromatography (Metrohm Model 850 Anion HP Gradient) with a Metrohm ASUPP7-250 (4 mm ID × 250 mm) column. All reagents and standards were prepared in ultrapure water (18 MΩ cm). The eluent solution was 3.2 mM Na_2CO_3 with 1.2 mM of $NaHCO_3$. The Metrohm Suppression Module (MSM) solutions were 100 mM sulfuric acid for regeneration and ultrapure water for rinsing. Cations were analyzed using an Agilent 8800 ICP-QQQ. All of the reagents and tuning solutions were procured from Agilent. Samples were acidified using 2% nitric acid before analysis. Alkalinity was measured using the Gran Function Plot Method available in U.S. Geological Survey online software [xviii].

Apparent molecular weight (AMW) of dissolved organic matter (DOM) was measured using size exclusion chromatography (SEC). High-performance liquid chromatography (HPLC) (Agilent 1290) hyphenated with an organic carbon detector (Suez GE Sievers M9 TOC analyzer) was used to measure dissolved organic carbon (DOC) at various AMWs. The separation column consisted of a hydroxylated methacrylic polymer (TOYOPEARL® HW-50S, Tosoh Bioscience LLC; 21 mm x 250 mm). Eluant was prepared with 4 mM phosphate buffer (pH 6.8) and 25 mM sodium sulfate.

500 µL samples were analyzed for 120 min. Polystyrene sulfonates with molecular weights (MWs) of 891, 3420, 6430, 15800, 33500, 65400 and 152000 Da were injected as MW standards (Polymer Standards Service, Mainz, Germany).

TOC and DOC were analyzed using a Shimadzu TOC-L CSH Total Organic Carbon Analyzer. Prior to acidification, samples were filtered with Micron 0.45 µm polyether sulfone disk filters using the method specified in Karanfil et al. [xix]. Approximately 10 mL of the samples were transferred into 20 mL glass vials for TOC and DOC analysis. Samples were then acidified to pH values lower than 3 using 35% hydrochloric acid (Fisher Scientific). Each sample and calibration curve point were measured up to five times by the instrument and the average of three non-outlier values were reported as the final results.

UV and fluorescence spectra were simultaneously measured via a Horiba Aqualog fluorometer (Horiba Scientific) scanning UV absorbance between 200 and 580 nm. Excitation-emission matrices (EEM) were obtained by scanning fluorescence from excitation wavelengths from 225 to 450 nm, and emission wavelengths from 250 to 580 nm. Corrections for inner filter effects were performed, and subsequently, light scattering including Rayleigh and Tyndall were removed using three-dimensional interpolation after subtracting the fluorescence spectra of Milli-Q water [xx]. Arbitrary units were converted to Raman units (RU) based on the integrated area of Raman peak of Milli-Q water [xxi]. All the EEM data processing and visualization were conducted using MATLAB R2018a (Mathworks) [xxii].

Scaling indices were calculated using the PHREEQC aqueous phase thermodynamic modeling package from the US Geological Survey [xxiii]. The PHREEQC model uses extended

Debye–Huckel and the Davies equations for modeling solution phase activity coefficients [23]. A Hach turbidity meter was used to measure the turbidity of the samples right after collection.

2.5 Parallel factor (PARAFAC) Analysis

Parallel factor analysis (PARAFAC) was conducted using drEEM toolbox downloaded at http://www.models.life.ku.dk/algorithms. The toolbox codes were analyzed using MATLAB (R2018a, version 9.4.0.813654). In total, 156 samples were used for PARAFAC analysis after the data points below 240 nm of excitation wavelength were excised.

2.6 RO Simulations

Reverse osmosis system analysis (ROSA) software [xxiv] was used to assess the effect of the FBCR operating pH on potential water recovery by reverse osmosis. The ROSA software simulates the water quality of the permeate and concentrate solutions from the input water quality. Wastewater at a pH value of 7 with conventional pretreatment and a silt density index < 5 was chosen as the nature of the feed water. A DOW Filmtec membrane for brackish water (BW30-400) was used in the simulations. Simulations were run for water treated by the UF process for the observed 60% recovery. Potential water recoveries were also calculated for FBCR treated water for scenarios limited by a calcite Langlier Saturation Index (LSI) of 1.8 and/or a SiO_2 supersaturation of 200%. With the use of antiscalants, these values are normally achievable without significant membrane fouling [xxv].

3. Results and Discussion

3.1. Fluidized Bed Crystallization Reactor

The FBCR was operated at pH values ranging from 10.5 to 12. Table 2 shows the effluent turbidity and the saturation index for a variety of scale-forming mineral species at the influent to the FBCR. The saturation index (SI) is defined as:

(1)

where a_i is the activity of ion i, ν_i is the stoichiometric coefficient for species i, and K_{sp} is the solubility product for the mineral dissolution reaction. For all pH values, there was an increase in turbidity after the FBCR, and it ranged from 0.2 to 0.5 NTUs. This may indicate the presence of heterogeneous nucleation of mineral solids, or may result from particle scouring in the fluidized bed. However, the increase in turbidity was approximately an order of magnitude smaller than that measured in a previous FBCR study, which ranged from 3.6 to 5.2 NTUs [xxvi].

Table 2. Turbidity values and saturation indices for secondary effluent and influent solutions to the FBCR.

Parameters	**Secondary Effluent**	**FCBR pH Value**			
		10.5	11	11.5	12
Turbidity (NTU)	1.1	1.4	1.4	1.3	1.6
Saturation Index (SI)					
$CaCO_3$ (calcite)	0.07	2.36	2.38	2.41	2.42
$CaSO_4$ (gypsum)	-1.39	-1.81	-1.86	-1.97	-2.10
$CaMg(CO_3)_2$ (dolomite)	-0.20	4.46	4.52	4.53	4.42
$BaSO_4$ (barite)	0.39	0.22	0.19	0.12	0.01
$Mg(OH)_2$ (brucite)	-5.67	1.40	1.36	2.23	3.02
$CaMg_3(CO_3)_4$ (huntite)	-5.08	4.31	4.45	4.42	4.07
$MgCO_3$ (magnesite)	-0.85	1.52	1.56	1.54	1.41

As shown in Table 2, only calcite and barite were supersaturated in the secondary effluent. However, the extents of supersaturation were significantly below those that lead to

homogeneous nucleation, which for calcite is ~1.7 [5]. Injection of the 0.1 M NaOH solution into the FBCR lowered the saturation indices for gypsum and barite due to both dilution and decreases in solution phase activity coefficients. By increasing the pH values to 11.5, the SI values increased for calcite, dolomite, huntite and magnesite, which is due to the increase in . However, the SI values decreased for gypsum, barite and brucite as a result of decreased activity coefficients associated with increasing ionic strength. The SI values leveled out or decreased for dolomite, brucite and magnesite when the pH of the stream was increased to 12. This results from conversion of to , and decreased activity coefficients. However, the SI value for brucite monotonically increased with pH since it is not affected by the concentration.

Figure 2 shows the Ca^{2+}, Mg^{2+} and SiO_2 removal at 4 different pH values. As shown in Table 2, dolomite and calcite had the highest saturation indices of potentially scale forming mineral species. The PHREEQC modeling indicated that calcium precipitated as calcium carbonate, and the measured Ca^{2+} removal reached 97% at pH 12. Magnesium was precipitated as magnesium carbonate, or incorporated into the crystal lattice of calcium carbonate at pH values >10.5 [5,6]. Magnesium also precipitated as $Mg(OH)_2$ at higher pH values, and Mg^{2+} removal reached >99.9% at pH 12.

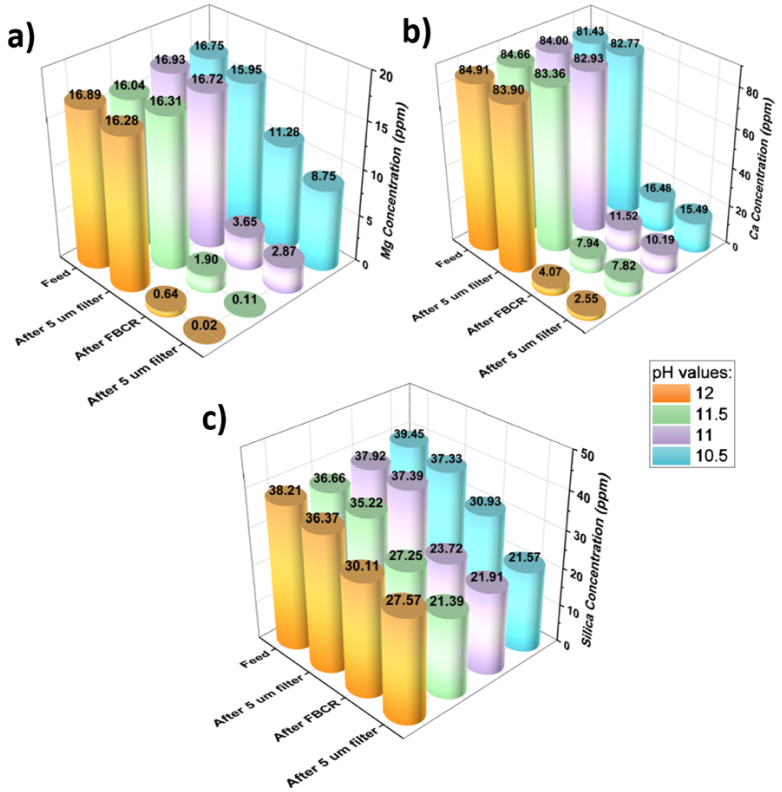

Figure 2. a) Mg^{2+}, b) Ca^{2+} and c) SiO_2 concentrations at different points in the treatment system for FBCR pH values between 10.5 and 12.

As shown in Figure 2c, dissolved silica was also removed in the FBCR. Previous studies have reported that dissolved silica is removed as $MgO(SiO_2)_x \cdot (H_2O)_x$ [xxvii]. Similar effluent silica concentrations were observed over the pH range 10.5 to 11.5, where 42-45% silica removal was observed. However, silica removal was lower at pH=12, which can likely be attributed to depletion of Mg^{2+} from the system due to increased $Mg(OH)_2$ precipitation.

A particularly important goal for pretreatment of secondary effluent is the removal of organic compounds. Figure 3 shows TOC concentrations at different points in the treatment system. TOC removal in the FBCR ranged from 7.4 to 25%, and increased with increasing pH value. TOC removal can occur via co-precipitation with calcium carbonate or magnesium

hydroxide, or by adsorption to mineral precipitates [6,15,16, xxviii]. Calcite has a highly structured rhombohedral shape and most often possess a negatively charged surface during softening. As shown in Figure 2, at a pH value of 10.5, there was a 7.4% reduction in TOC. Although the negative surface charge of calcite was unfavorable for adsorption of negatively charged NOM, incorporation of magnesium in the calcium carbonate crystal can result in a positive surface charge (or reduced negative charge) on the calcite precipitates [6]. Therefore, a small amount of NOM removal was seen at pH 10.5. By increasing the pH to higher values, $Mg(OH)_2$ precipitation became favorable. $Mg(OH)_2$ forms positively-charged noncrystalline precipitates with higher surface area compared to calcite [6]. This may explain the higher NOM removals (25%) at a pH value of 12. Furthermore, at high pH values, $CaOH^+$ and $MgOH^+$ formation may also contribute to direct precipitation of calcium or magnesium humate or fulvate [6].

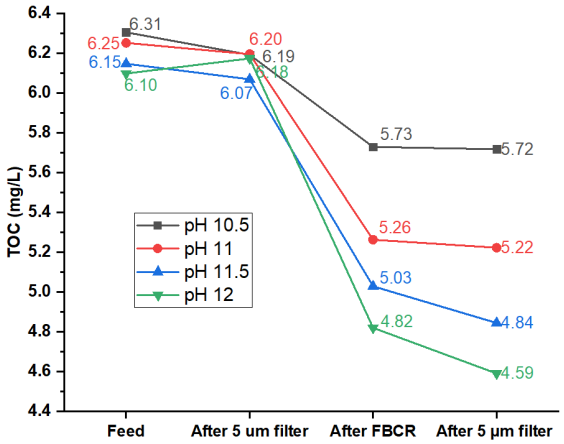

Figure 3. TOC concentrations at different points in the treatment system for FBCR pH values ranging from 10.5 to 12.

TOC concentrations determined via size exclusion chromatography are shown in Figure 4 for different points in the system. After the FBCR, there was an overall trend of organic carbon reduction with increasing pH, which is in accordance with the TOC data. Considering pH values of 10.5 and 11, there was an approximately even reduction in all 3 peaks at pH 10.5, while there was slightly higher reduction in the lower molecular weight peak for pH 11. At pH values of 11.5 and 12, SEC-OCD results show that the high molecular weight fraction of TOC in the *after FBCR* samples are substantially higher than those taken after the 5 µm filter. This suggests that the NOM is associated with particulate matter produced at pH values of 11.5 and 12. These pH values are where $Mg(OH)_2$ precipitation occurs. This suggests that NOM removal at pH values of 11.5 and 12 occurs via co-precipitation with $Mg(OH)_2$.

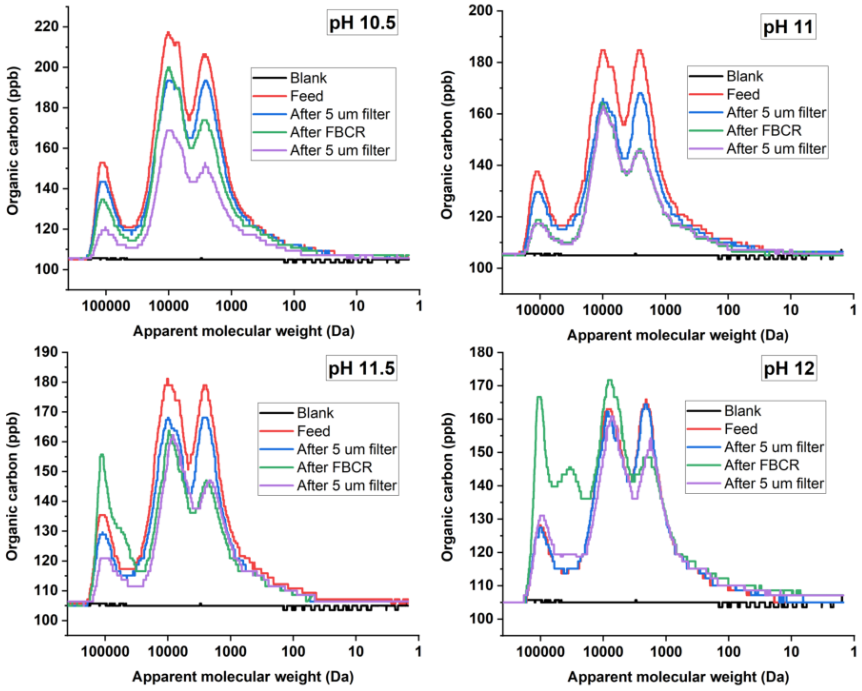

Figure 4. SEC-OCD results for SE treated by FBCR at different pH values.

3.2 EEM Spectra

EEM data can be used to provide insight into the types of NOM removed in the FBCR. A recently refined technique that combines EEM spectra and parallel factor data analysis is a valuable tool for characterizing NOM, and tracing its origins in aquatic samples [xxix]. EEM spectra of the water samples at different points in the treatment system are shown in Figure S1 in the Supporting Information. A series of PARAFAC models from 3 to 7 components were analyzed with non-negative constraints and subsequently validated using a split-half analysis with $S_3C_3T_3$. (Splits: 3, Combinations: 3, Tests: 3) [xxx,xxxi]. Among the models tested, 2, 3 and 5 component models passed the split half validation. A five component model was finally selected and its results are reported in Table 3 and Figure S2 in the Supporting Information. The fluorescence spectra of these five components show a resemblance to organic fluorophores by having multiple excitation maxima for a single emission maxima [xxxii].

Table 3. PARAFAC NOM component identification.

Component of this study	**Excitation/Emission wavelength**	**Description and probable source of the component (Reference)**
C1	255 (350)/420	Common to a wide range of freshwater environments, anthropogenic humic fluorophore group, (C6), <250 (320)/400 [29] Terrestrial humic substances, (P8), <260 (355)/434 [27] ADDIN EN.CITE Terrestrial humic substances, (C5), 250 (340)/440 [ ]
C2	<250 (350/440)	Terrestrial/autochthonous fulvic acid fluorophore group, (C4), <250 (360)/440 [29]
C3	260 (390)/492	Terrestrial humic substances, widespread, (P3), <260 (380)/498 [27]

		Terrestrial humic substances, (C1), 260 (360)/480 [30] Terrestrial humic substances, (C3), 270 (360)478 [26]
C4	<250 (320)/390	Marine and terrestrial humic substances, (C6), <250 (300)/406 Microbial humic, (C4), <250 (305)/390 [xxxiv]
C5	<250 (275)/340	Tryptophan-like, protein-like, (Peak T type) [xxxv] amino acids, free or bound in proteins, (P7), 280/342 [27] amino acids, free or protein bound, (C4), <250 (290)/360

According to Table 3, three of five components are humic-like substances. Comparing the EEM maxima spectra of C4 with C1, components C1 has a higher excitation wavelength for an approximately similar emission wavelength. Excitation at higher wavelength for C1 shows that the fluorophores responsible for this contain several functional groups or have higher aromaticity [xxxvi]. Comparing C1 with C3 humic substances, component 3 has longer emission wavelength compared to C1. This might be due to the presence of more conjugated fluorescing molecules in C3 compared to C1. Component 5 is identified as tryptophan-like protein in several studies cited in Table 3.

Figure 5 shows the maximum fluorescence intensity (F_{max}) values for different pH conditions in the FBCR. As shown in Figure 5a, the FBCR was able to reduce the F_{max} value for all five components, removing 7% of C1, 100% of C2, 55% of C3, 40% of C4 and 44% of C5. Component 1 shows the lowest removal among the five groups. Compared to C3, C1 has more functional groups that are deprotonated at high pH values which results in high negative charges for these components. As shown in Figure 5a, there was no removal for this component until pH values above 11.5, which might be due to precipitation of $Mg(OH)_2$, which possesses a highly

positive surface charge.

For comparison purposes, NOM removal by UF and $FeCl_3$ was also investigated. NOM removal data by UF is shown in Table S1 and EEM spectra for UF feed permeate, and backwash are shown in Figure S3. Data for NOM removal by $FeCl_3$ is shown in Figure S4 and EEM spectra for the $FeCl_3$ treated water is shown in Figure S5. The F_{max} data in Figure 5b shows slight to no removal for components 1 to 4 by UF. This is due to the fact that these components are too small to be filtered by the membrane. However, UF was able to remove approximately 11% of component 5, which consists of large amino acid molecules. Overall, UF was able to remove approximately 18% of the TOC in the secondary effluent water. As shown in Figure 5c, the $FeCl_3$ was able to remove all 5 NOM components, with up to 40% of C1, 38% of C2, 65% of C3, 34% of C4 and 26% of C5. Overall, coagulation by $FeCl_3$ was able to remove 49% of TOC at the optimal dose of 45 mg/L as Fe (Figure S5). This is substantially greater TOC removal than the 25% removal in the FBCR at a pH value of 12.

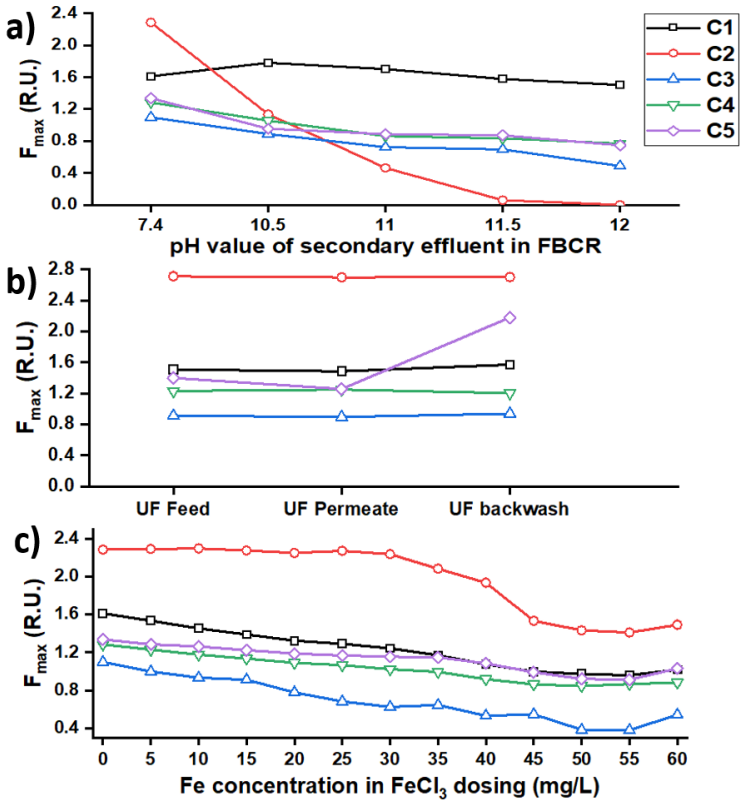

Figure 5. F_{max} values for different conditions in: a) FBCR, b) UF and c) $FeCl_3$ coagulation/flocculation.

3.3 FBCR Effect on RO Recovery

The effect of the FBCR on the water recovery obtainable in a subsequent RO process was calculated using ROSA simulation software. Table 4 shows the saturation indices for compounds that may cause membrane scaling. As the RO system is currently operated, $BaSO_4$ has the highest saturation index of potentially scale forming minerals. Thus, it is likely that $BaSO_4$ has limited the RO recovery to only 60% using UF pretreatment. Also shown in Table 4 are the saturation indices for water treated by FBCR at pH values from 10.5 to 12. The recovery for these simulations was determined by restricting the LSI to ≤ 1.8, and the SiO_2 supersaturation ≤ 200% [25]. For all FBCR pH values, the $BaSO_4$ saturation index was less than that for the UF pretreatment. Potential

recoveries with pretreatment via the FBCR ranged from 93 to 97%. For the lowest recovery of 93%, this represents a factor of 5.7 reduction in the volume of concentrate solution as compared to pretreatment using UF. This analysis does not include RO recovery being limited by membrane fouling by organic matter. However, pretreatment by the FBCR removed nearly twice as much NOM as UF pretreatment. In addition, membrane fouling by NOM is exacerbated by Ca^{2+} [xxxvii]. Thus, removal of 82-97% of the Ca^{2+} in the FBCR is expected to lower membrane fouling by NOM.

Table 4. Concentrations of Mg^{2+}, Ca^{2+}, and Ba^{2+} in simulated RO concentrate solutions along with saturation indices and supersaturation % for potentially scale-forming species. Also shown are the recovery % for each simulation with different pretreatment.

4. Conclusions

This study investigated the effectiveness of using a FBCR as a pretreatment process for reverse osmosis reclamation of secondary effluent wastewater. The FBCR was effective at

removing scale-forming minerals, but was only half as effective as $FeCl_3$ for removing NOM. Interestingly, UF – a technology often recommended as RO pretreatment for water reuse applications – showed the least NOM removal. In the FBCR, the highest levels of NOM removal occurred at the highest pH values, where $Mg(OH)_2$ precipitation occurs. The FBCR was also able to attenuate all five NOM components, and removed 100% of the autochthonous fulvic acids, which are produced by algae and bacteria. Removal of autochthonous fulvic acids may be an important consideration in water reuse applications since they are likely to comprise a significant fraction of the total NOM.

Although fluidized bed crystallization has several advantages over conventional lime softening, such as: shorter hydraulic detention time, reduced chemical usage, no $Mg(OH)_2$ settling issues, and elimination of sludge production, the maximum 25% NOM removal in the FBCR was less than that normally observed for conventional lime softening [7]. In addition, $FeCl_3$ is often added during conventional lime softening to improve NOM removal. $FeCl_3$ addition to a FBCR is not likely to be effective, since the process effluent is at a high pH where NOM adsorption to ferric hydroxide is greatly reduced. Thus, if high levels of NOM removal are required prior to reverse osmosis, a separate coagulation step would be recommended after neutralization of the effluent from the FBCR.

Acknowledgements

Authors would like to thank the National Science Foundation (PFI: AIR-TT: 1640445) for providing the funding for this work. We also acknowledge Mr. Shawn Beitel from University of

Arizona for facilitating the use of the instruments, and Agilent Technologies for their continued technical and equipment support to the Snyder Research Lab. Funding sources had no role in the research activities or in the preparation of this manuscript.

Declaration of interests: none.

5. References

[i] Service, R.F., 2006. Desalination freshens up. Science 313, 1088-1090. http://dx.doi.org/10.1126/science.313.5790.1088.

[ii] Gerrity, D., Pecson, B., Trussell, R.S., Trussell, R.R., 2013. Potable reuse treatment trains throughout the world. J Water Supply Res T 62, 321-338. http://dx.doi.org/10.2166/aqua.2013.041.

[iii] Warsinger, D.M., Chakraborty, S., Tow, E.W., Plumlee, M.H., Bellona, C., Loutatidou, S., Karimi, L., Mikelonis, A.M., Achilli, A., Ghassemi, A., Padhye, L.P., Snyder, S.A., Curcio, S., Vecitis, C.D., Arafat, H.A., Lienhard, V.J.H., 2018. A review of polymeric membranes and processes for potable water reuse. Prog Polym Sci 81, 209-237. http://dx.doi.org/10.1016/j.progpolymsci.2018.01.004.

[iv] Rahardianto, A., Gao, J.B., Gabelich, C.J., Williams, M.D., Cohen, Y., 2007. High recovery membrane desalting of low-salinity brackish water: Integration of accelerated precipitation softening with membrane RO. J Membrane Sci 289, 123-137. http://dx.doi.org/10.1016/j.memsci.2006.11.043

[v] Graveland, A., Vandijk, J.C., Demoel, P.J., Oomen, J.H.C.M., 1983. Developments in Water Softening by Means of Pellet Reactors. J Am Water Works Ass 75, 619-625.

[vi] Russell, C.G., Lawler, D.F., Speitel, G.E., 2009. NOM coprecipitation with solids formed during softening. J Am Water Works Ass 101, 112.

[vii] Davis, M.L. Water and Wastewater Engineering, McGraw-Hill, New York, 2010, pp. 4-20.

[viii] Rahardianto, A., McCool, B.C., Cohen, Y., 2010. Accelerated desupersaturation of reverse osmosis concentrate by chemically-enhanced seeded precipitation. Desalination 264, 256-267. http://dx.doi.org/10.1016/j.desal.2010.06.018

[ix] Sluys, J.T.M., Verdoes, D., Hanemaaijer, J.H., 1996. Water treatment in a membrane-assisted crystallizer (MAC). Desalination 104, 135-139. http://dx.doi.org/10.1016/0011-9164(96)00036-7

[x] Racar, M., Dolar, D., Spehar, A., Kras, A., Kosutic, K., 2017. Optimization of coagulation with ferric chloride as a pretreatment for fouling reduction during nanofiltration of rendering plant secondary effluent. Chemosphere 181, 485-491. http://dx.doi.org/10.1016/j.chemosphere.2017.04.108

[xi] Voutchkov, N., 2017. Pretreatment for Reverse Osmosis Desalination. Elsevier.

[xii] Ishida, K.P., Cooper, W.J., 2015. Analysis of Parameters Affecting Process Efficiency, Energy Consumption, and Carbon Footprint in Water Reuse. WateReuse Research Foundation.

[xiii]Pearce, G.K., 2008. UF/MF pre-treatment to RO in seawater and wastewater reuse applications: a comparison of energy costs. Desalination 222, 66-73. http://dx.doi.org/10.1016/j.desa1.2007.05.029

[xiv] Aghdam, M.A., Zraick, F., Simon, J., Farrell, J., Snyder, S.A., 2016. A novel brine precipitation process for higher water recovery. Desalination 385, 69-74. http://dx.doi.org/10.1016/j.desal.2016.02.007

[xv] Liao, M.Y., Randtke, S.J., 1985. Removing Fulvic-Acid by Lime Softening. J Am Water Works Ass 77, 78-88.

[xvi] Randtke, S.J., Thiel, C.E., Liao, M.Y., Yamaya, C.N., 1982. Removing soluble organic contaminants by lime-softening. Journal - American Water Works Association 74, 192-202. http://dx.doi.org/10.1002/j.1551-8833.1982.tb04888.x

[xvii] Benefield, L.D., Morgan, J.M. Chemical Precipitation, in R.D. Letterman (ed), Water Quality and Treatment, 5th Ed., American Water Works Association, McGraw-Hill, New York, 1999, pp. 9.1-9.91.

[xviii] USGS, 2013 https://or.water.usgs.gov/alk/download.html (accessed 9-19-2019)

[xix] Karanfil, T., Erdogan, I., Schlautman, M.A., 2003. Selecting filter membranes for measuring DOC and UV254. J Am Water Works Ass 95, 86-100.

[xx] Park, M., Snyder, S.A., 2018. Sample handling and data processing for fluorescent excitation -emission matrix (EEM) of dissolved organic matter (DOM). Chemosphere 193, 530-537. http://dx.doi.org/10.1016/j.chemosphere.2017.11.069

[xxi] Zepp, R.G., Sheldon, W.M., Moran, M.A., 2004. Dissolved organic fluorophores in southeastern US coastal waters: correction method for eliminating Rayleigh and Raman scattering peaks in excitation-emission matrices. Mar Chem 89, 15-36. http://dx.doi.org/10.1016/j.marchem.2004.02.006

[xxii] Murphy, K.R., Stedmon, C.A., Graeber, D., Bro, R., 2013. Fluorescence spectroscopy and multi-way techniques. PARAFAC. Anal Methods-Uk 5, 6557-6566. http://dx.doi.org/10.1039/c3ay41160e

[xxiii] Parkhurst, D.L., Appelo, C.A.J., 2013. Description of input and examples for PHREEQC version 3—a computer program for speciation, batch-reaction, one-dimensional transport, and inverse geochemical calculations. U.S. Geological Survey Techniques and Methods.

[xxiv] Reverse Osmosis System Analysis Software, DOW Filmtec, https://www.desalitech.com/rosa_download_lp/

[xxv] Lenntech, Hydranautics RO Water Chemistry, https://www.lenntech.com/Data-sheets/Hydranautics-RO-Water-Chemistry-LL.pdf

[xxvi] Harms, W.D., Robinson, R.B., 1992. Softening by Fluidized-Bed Crystallizers. J Environ Eng-Asce 118, 513-529. http://dx.doi.org/10.1061/(Asce)0733-9372(1992)118:4(513)

[xxvii] Stanford, B.; Leising, J. F.; Bond, R.; Snyder, S. A. Inland desalination: Current practices, environmental implications, and case studies in Las Vegas, NV. In Sustainability Science and Engineering, Vol. 2. I. C. Escobar and A. I. Schafer, eds. Elsevier, Amsterdam, 2010.

[xxviii] Gerwe, C.E., 2003. Natural Organic Matter Adsorption Onto and Coprecipitation With Solids Formed During Softening, Civil, Architectural, and Environmental Engineering. University of Texas, Austin.

[xxix] Stedmon, C.A., Markager, S., Bro, R., 2003. Tracing dissolved organic matter in aquatic environments using a new approach to fluorescence spectroscopy. Mar Chem 82, 239-254. http://dx.doi.org/10.1016/S0304-4203(03)00072-0

[xxx] Murphy, K.R., Stedmon, C.A., Waite, T.D., Ruiz, G.M., 2008. Distinguishing between terrestrial and autochthonous organic matter sources in marine environments using fluorescence spectroscopy. Mar Chem 108, 40-58. http://dx.doi.org/10.1016/j.marchem.2007.10.003

[xxxi] Sanchez, N.P., Skeriotis, A.T., Miller, C.M., 2014. A PARAFAC-Based Long-Term Assessment of DOM in a Multi-Coagulant Drinking Water Treatment Scheme. Environ Sci Technol 48, 1582-1591. http://dx.doi.org/10.1021/es4049384

[xxxii] Stedmon, C.A., Markager, S., 2005. Resolving the variability in dissolved organic matter fluorescence in a temperate estuary and its catchment using PARAFAC analysis. Limnol Oceanogr 50, 686-697. http://dx.doi.org/10.4319/lo.2005.50.2.0686

[xxxiii] Baghoth, S.A., Sharma, S.K., Amy, G.L., 2011. Tracking natural organic matter (NOM) in a drinking water treatment plant using fluorescence excitation-emission matrices and PARAFAC. Water Res 45, 797-809. http://dx.doi.org/10.1016/j.watres.2010.09.005

[xxxiv] Yamashita, Y., Jaffe, R., 2008. Characterizing the interactions between trace metals and dissolved organic matter using excitation-emission matrix and parallel factor analysis. Environ Sci Technol 42, 7374-7379. http://dx.doi.org/10.1021/es801357h

[xxxv] Coble, P.G., 1996. Characterization of marine and terrestrial DOM in seawater using excitation emission matrix spectroscopy. Mar Chem 51, 325-346. http://dx.doi.org/10.1016/0304-4203(95)00062-3

[xxxvi] Coble, P.G., Del Castillo, C.E., Avril, B., 1998. Distribution and optical properties of CDOM in the Arabian Sea during the 1995 Southwest Monsoon. Deep-Sea Res Pt Ii 45, 2195-2223. http://dx.doi.org/10.1016/S0967-0645(98)00068-X

[xxxvii] Hong, S., Elimelech, M., 1997. Chemical and physical aspects of natural organic matter (NOM) fouling of nanofiltration membranes. J Mem Sci 132, 159-181. https://doi.org/10.1016/S0376-7388(97)00060-4